Optimal Flux Selection of an Induction Machine for Maximum Torque Operation in Flux-Weakening Region

Jul-Ki Seok, *Student Member, IEEE,* and Seung-Ki Sul, *Member, IEEE*

***Abstract*—The optimal flux-searching algorithms of an induction machine have reached a stage of development permitting maximum torque operation over an entire flux-weakening region. In the high-speed region, however, the sensitivity to parameter errors of an induction machine still remains a problem. This paper presents an approach that ensures maximum torque operation maintaining robustness to parameter error in the flux-weakening region. To guarantee the performance in the high-speed region, the machine leakage inductance is adapted on line, based on the injection of sinusoidal current. Also, the detuned effect on machine inductance is thoroughly analyzed to relate the sensitivity of parameters to the performance of the flux-weakening region. Experimental results demonstrate that the proposed adaptation scheme effectively selects the optimal flux level regardless of variation of leakage inductance.**

***Index Terms*—Flux-weakening, induction machine.**

I. Introduction

CONSTANT power operation of a general flux-oriented induction machine drive is becoming increasingly attractive in a wide variety of speed control applications such as spindle, traction, and electric vehicle drive. Also, in the modern industrial fields, in order to improve plant productivity, the constant power range of drive should be extended as wide as possible. In these high-speed applications, however, the maximum output torque and power developed by the machine are ultimately dependent on the allowable inverter current and the maximum voltage rating which the inverter can supply to the machine. Therefore, considering the limited voltage and current capacities, it is desirable to use a control scheme that yields the maximum torque per ampere over the whole speed range. In this point of view, some studies [1], [2] have been reported to guarantee the maximum torque in the flux-weakening region. In these strategies, a closed-loop voltage controller sets the flux reference and this scheme is robust against machine parameter variations. However, some stimulations in the voltage controller are initiated by speed control and can disturb the voltage control severely because of its poor dynamic properties [2]. Therefore, this control strategy is not appropriate for low-inertia machine drive or rapid speed changing applications. Other approaches [3], [4] have developed the analytic solution of the flux reference for producing the maximum torque in the flux-weakening region. In these strategies, the flux reference and the onset of the flux-weakening region can be achieved by using the machine parameters. Using accurate machine parameter data, these schemes yield faster dynamic performance than the closed-loop voltage controller method and the produced torque is almost same as that of the voltage controller method. Compared to any other approaches [1]–[4], our earlier work [5] has shown that the significant increase of available torque can be achieved in the flux-weakening region by incorporating rotor flux dynamics into limited inverter conditions. Unfortunately, this approach also requires that accurate machine inductance data should be available to calculate onset of flux-weakening region and optimal stator current trajectory.

This paper demonstrates the detuned effect of machine inductance on maximum torque operation in the flux-weakening region. Examining the detuned effect of machine inductance, it is known that the flux-weakening performance has a relatively low sensitivity to magnetizing inductance detuning and a high sensitivity to stator transient inductance detuning.

Generally, the stator transient inductance can be obtained by impressing single-phase pulsing on the induction machine and measuring the elapsed time between preset values of current [6], [7]. But this transient test yields an estimate of the machine's transient inductance that is consistently lower than the actual value [8]. This is because skin effects corrupt the high-frequency measurements of stator transient inductance.

In addition, saturation due to both induced-rotor currents and main flux severely impacts the stator transient inductance [9]. In this point of view, some investigations were devoted to the on-line adaptation of stator transient inductance [10], [11]. In these studies, the harmonic component with high frequency apart from operating frequency is intentionally superimposed on the voltage or current command. These schemes are almost insensitive to other parameters and easily implemented only using a digital filter with bandpass or low-pass characteristics. However, the values obtained from these schemes are also consistently lower due to skin effects. This means that parameters estimated from high-frequency excitation signal would not be suitable for covering all operating conditions. In this point of view, an approach which constraints the excitation frequency to minimize skin effect was presented [8]. However, this approach paid very little attention to the estimation of

Manuscript received January 1, 1998; revised August 19, 1998. Recommended by Associate Editor, O. Ojo.

J.-K. Seok is with the Production Engineering Center, FA Research Institute, Samsung Electronics Company Ltd., Suwon City, Korea.

S.-K. Sul is with the School of Electrical Engineering, Seoul National University, Seoul, Korea.

Publisher Item Identifier S 0885-8993(99)05561-1.

0885–8993/99$10.00 © 1999 IEEE

stator transient inductance in conjunction with the operation over the wide range of flux weakening.

To compensate the stator transient inductance detuning in overall speed region, an on-line adaptation scheme based on the signal injection method is proposed in this paper. The corrupting influence of skin effect on stator transient inductance is demonstrated and its effect on system performance is investigated. The adaptation procedure intends to reduce the adverse effects of skin effect on the estimation of the stator transient inductance and the influence of detuning on other machine parameters.

II. Voltage and Current Constraints

As widely known, the maximum output torque developed by the machine is limited by allowable voltage and current ratings of the machine and those of inverter. The machine torque T_e and the rotor flux λ_{dr}^e of the rotor flux-oriented induction machine in synchronously rotating reference frame can be expressed as

$$\lambda_{dr}^e = \frac{L_m}{1+p\tau_r} i_{ds}^e \tag{1}$$

$$T_e = \frac{3}{4} P \frac{L_m}{L_r} \lambda_{dr}^e i_{qs}^e. \tag{2}$$

In the above equation, τ_r is the rotor time constant, p represents the differential operator, and P indicates the number of poles. L_m and L_r represent the magnetizing inductance and rotor inductance, respectively.

Neglecting the stator resistance voltage drop for high-speed operation, the d–q-axis stator voltages in the synchronous reference frame become

$$V_{qs}^e \cong \omega_e \left(\frac{L_m}{L_r} \lambda_{dr}^e + L_\sigma i_{ds}^e \right) \tag{3}$$

$$V_{ds}^e \cong -\omega_e L_\sigma i_{qs}^e. \tag{4}$$

The maximum stator voltage $V_{s\ \max}$ is determined by the available dc-link voltage and the pulsewidth modulation (PWM) strategy and must satisfy the following condition:

$$V_{qs}^{e^2} + V_{ds}^{e^2} \le V_{s\ \max}^2. \tag{5}$$

The maximum stator current $I_{s\ \max}$ is also limited by the inverter current rating as well as the thermal rating of the induction machine. Hence, the d–q-axis currents must also satisfy the following limit condition:

$$I_{qs}^{e^2} + I_{ds}^{e^2} \le I_{s\ \max}^2. \tag{6}$$

III. Optimal Flux for Maximum Torque Capability

According to the control scheme, no closed-loop flux control is used but the reference of the d-axis current is established directly by the flux reference. That is why the step response of the rotor flux can be calculated very easily from the first-order differential (1) as far as the current is assumed to track its reference instantaneously $i_{ds}^{e^*} = i_{ds}^e$. Rotor flux and machine torque result as

$$\lambda_{dr}^e = L_m I_{ds}^{e^*} + \alpha e^{-(t/\tau_r)} \tag{7}$$

where $\alpha = \lambda_{dro}^e - L_m i_{ds}^e$.

In (7), λ_{dro}^e and i_{ds}^e is the value of the rotor flux and d-axis current at a sampling instant

$$T_e = \frac{3}{2} P \frac{L_m}{L_r} (L_m i_{ds}^{e^*} + \alpha e^{-(t/\tau_r)}) i_{qs}^e. \tag{8}$$

At steady state, the second term in (7) decreases steadily and (7) satisfy the steady-state condition of rotor flux as

$$\lambda_{dr}^e = L_m i_{ds}^{e^*}. \tag{9}$$

By combining (1)–(7), the optimal stator currents of the flux-weakening region I are determined as (10), given at the bottom of the page, and

$$i_{qs}^{e^*} = \sqrt{I_{s\ \max}^2 - i_{ds1}^{e^{*2}}} \tag{11}$$

where $\delta = (L_m/L_r)\alpha e^{-(t/\tau_r)}$.

L_s and L_σ represent the stator inductance and stator transient inductance, respectively.

In the flux-weakening region I [1], the slip angular velocity increases as the machine speed is increased. As the speed is further increased, the slip reaches the maximum value due to the voltage constraint, and then the region II. In the flux-weakening region II, the voltage limit is only considered to obtain maximum achievable torque [4]. Combining (3)–(5) and (8), the torque can be rearranged as

$$T_e = \frac{3}{2} P \frac{L_m}{L_r} \frac{\sqrt{(V_{s\ \max}/\omega_e)^2 - (L_s i_{ds}^{e^*} + \delta)^2}}{L_\sigma} \cdot (L_m i_{ds}^{e^*} + \alpha e^{-(t/\tau_r)}). \tag{12}$$

To maintain maximum torque operation in this region, the optimal currents of the flux-weakening region II can be calculated from the condition $(dT_e/di_{ds}^{e^*}) = 0$ as (13) and (14)

$$i_{ds}^{e^*} = \frac{-b + \sqrt{b^2 - 4ac}}{2a} \tag{13}$$

where $a = 2L_m L_s^2$, $b = L_s^2 \alpha e^{-(t/\tau_r)} + 3L_m L_s$, and $c = L_s \delta \alpha e^{-(t/\tau_r)} + L_m \delta^2 - L_m (V_{s\ \max}/\omega_e)^2$

$$i_{qs}^{e^*} = \frac{\sqrt{(V_{s\ \max}/\omega_e)^2 - (L_s i_{ds2}^e + \delta)^2}}{L_\sigma}. \tag{14}$$

$$i_{ds}^{e^*} = \frac{-L_s\delta + \sqrt{(L_s\delta)^2 + (L_s^2 - L_\sigma^2)((V_{s\ \max}/\omega_e)^2 - \delta^2 - L_\sigma^2 I_{s\ \max}^2)}}{L_s^2 - L_\sigma^2} \tag{10}$$

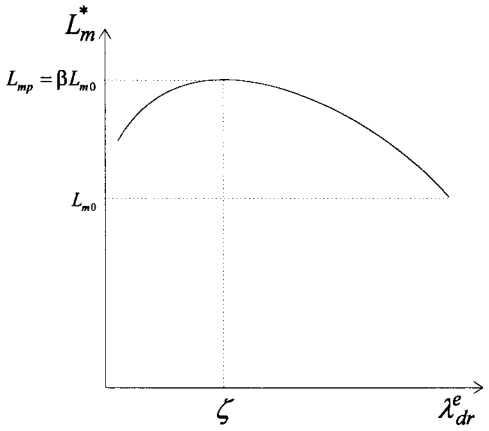

Fig. 1. Trajectory of simple magnetizing inductance model.

For the computation of onset of flux-weakening region and optimal stator currents, the inductance values of machine under consideration should be used. If incorrect inductance values are used in the controller, it may cause instantaneous errors in flux level resulting in sluggish dynamics or catastrophic breakdown due to the loss of current regulation. Thus, it is essential to identify accurate inductance values of machine in order to achieve the ideal maximum torque operation in the flux-weakening region.

IV. Machine Inductance Detuned Effect During Flux-Weakening Region

A. Detuned Effect of Magnetizing Inductance

Generally, it should be noted that the magnetizing curve of the induction machine can be obtained from the no-load test, if the stator voltage V_s and stator current I_s are determined. By plotting V_s as a function of I_s, the magnetizing curve can also be plotted to give the variation of L_m with rotor flux λ_{dr}^e.

To examine the detuned effect of magnetizing inductance, a simple model which is useful for representing the variation of magnetizing inductance is shown in Fig. 1 and (15)

$$L_m^* = \gamma(\lambda_{dr}^e - \zeta)^2 + L_{mp}. \tag{15}$$

In such a case, the implied relationship is

$$\frac{L_{mp}}{L_{s0}} \cong \frac{L_{mp}}{L_{m0}} = \beta. \tag{16}$$

Note that factor β represents the aspect of controller maximum mismatch due to incorrect controller value L_{m0} in the flux-weakening region. In (10) and (13), the order of magnetizing inductance is equal in the denominator and the nominator, and this means that the detuned effect of magnetizing inductance is canceled to some extent. Therefore, the effect on detuning is rather small and the control scheme has an inherent self-compensating property for the change of the magnetizing inductance.

In the case of the machine in Table I, it is known that ζ is 0.3 and β is 1.15 from no-load test data. In order to consider a more severe situation, for a value of ζ and β which is chosen as 0.3 and 1.5, some tests are performed and the result is shown in Fig. 2. In this figure, it is shown that the rotor flux under tuned condition is very close to that under detuned condition during all flux-weakening region. This figure clearly offers the evidence of the inherent self-compensating property for the change in magnetizing inductance in the flux-weakening region. Therefore, the optimal flux-weakening scheme has a robustness to the magnetizing inductance variation, and it is unnecessary to perform tedious no-load tests in order to obtain the magnetizing curve in the flux-weakening operation.

TABLE I
Ratings and known parameters of induction machine under test

Rated power output	22 kW
Rated line voltage	220V
Number of pole	4
Supply frequency	60 Hz
Stator resistance	0.04 Ω
Rotor resistance	0.024 Ω
Magnetizing inductance	13.24 mH
Stator transient inductance	1.1 mH
Moment of inertia	0.16 $Kg \cdot m^2$

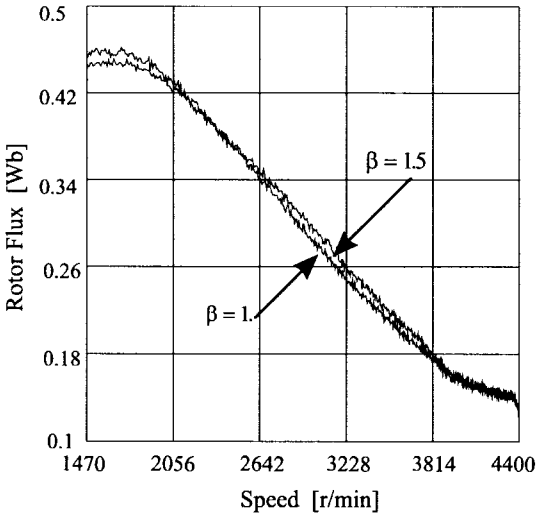

Fig. 2. Rotor flux for tuned ($\beta = 1$) and detuned ($\beta = 1.5$) magnetizing inductance.

B. Detuned Effect of Stator Transient Inductance

The rotor flux must be calculated from the stator or air-gap flux by employing the machine leakage inductance. Therefore, the optimal flux selection algorithm is affected by the errors on the stator transient inductance. Fig. 3 shows the detuned effects of leakage inductance for the rotor flux selected by the optimal flux selection algorithm. When the estimated leakage inductance is lower than actual one by 20%, the machine is operated at a reduced rotor flux with decreased torque capability at high speed. On the other hand, when the leakage inductance is overestimated by 20%, the machine is operated at an increased flux level. In this case, the inverter runs out

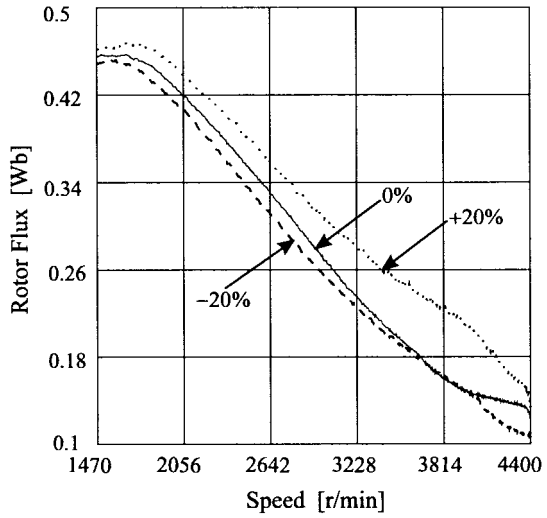

Fig. 3. Rotor flux for tuned and detuned transient leakage inductance.

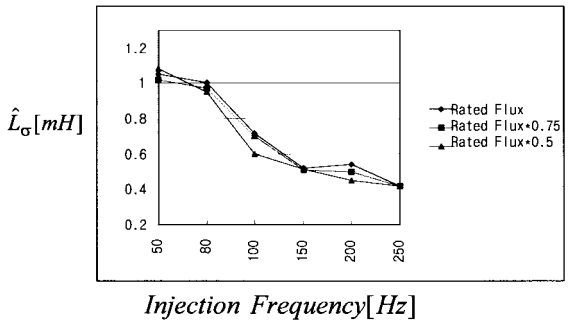

Fig. 4. Stator transient inductance according to injected frequency.

of voltage, and the current regulation is lost. Therefore, to perform robust maximum torque control at high speed, the stator transient inductance should be adapted on line.

V. Stator Transient Inductance Identification

The harmonic component is often superimposed on the controller command to estimate the stator transient inductance. However, the estimated values obtained from harmonic frequency method may be consistently lower due to skin effect. To investigate the influence of injected harmonic frequency, some tests are performed on the machine in Table I. Fig. 4 shows the stator transient inductance obtained by harmonic frequency method [10], [11] at various flux levels. In this test, the frequency of injection signal in the synchronous rotating reference frame is selected between 50 and 250 Hz. As the excitation frequency increases, the estimated stator transient inductance decreases due to skin effect. Therefore, to minimize skin effect on stator transient inductance estimation, the frequency of injected signal should be selected carefully.

The d-axis current is controlled in the synchronously rotating reference frame according to the following relationship:

$$i^{e^*}_{ds\_id} = i^{e^*}_{ds} + I_h \sin\omega_h t = i^{e^*}_{ds} + \tilde{i}^{e}_{ds}. \tag{17}$$

On the d axis, an optimal d-axis current $i^{e^*}_{ds}$ with injected sinusoidal term $I_h \sin\omega_h t$ is applied. Here, $i^{e^*}_{ds}$ is the output reference current of flux-weakening controller in (10) and (13).

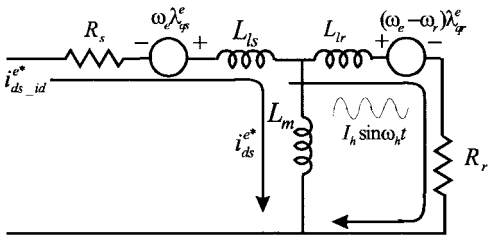

Fig. 5. D-axis equivalent circuit for stator transient inductance identification.

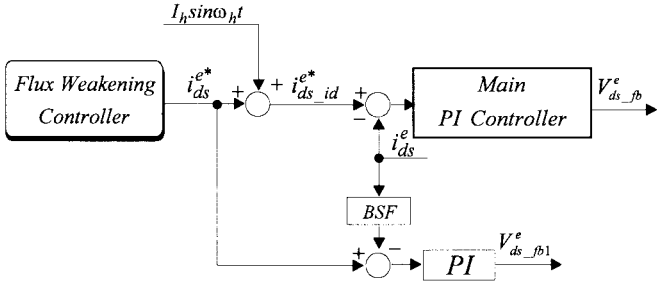

Fig. 6. Voltage component calculation of flux-weakening controller.

The sinusoidal current $I_h \sin\omega_h t$ has a constant frequency ω_h and amplitude I_h that do not produce net torque. When the frequency ω_h is high enough, most of the sinusoidal current $\tilde{i}^e_{ds}$ flows through the rotor branch as shown in Fig. 5. With given machine parameters obtained from name plate data, the frequency ω_h is determined using the following condition:

$$\frac{|R_r + j\omega_h L_{lr}|}{|j\omega_h L_m|} \le 0.05. \tag{18}$$

Then, the d-axis current controller output voltage $V^e_{ds\_fb}$ consists of the flux-weakening controller voltage component $V^e_{ds\_fb1}$ and ripple voltage component $\tilde{V}^e_{ds\_fb}$ as

$$V^e_{ds\_fb} \cong L_\sigma\left(\frac{di^{e^*}_{ds}}{dt} + \frac{d\tilde{i}^e_{ds}}{dt}\right) = V^e_{ds\_fb1} + \tilde{V}^e_{ds\_fb}. \tag{19}$$

The ripple voltage component $\tilde{V}^e_{ds\_fb}$ in (19) includes the information of stator transient inductance as

$$\begin{aligned}\tilde{V}^e_{ds\_fb} &= (R_s + R_r) I_h \sin\omega_h t + \omega_h (L_{ls} + L_{lr}) \cos\omega_h t \\ &\cong (R_s + R_r) I_h \sin\omega_h t + \omega_h L_\sigma I_h \cos\omega_h t.\end{aligned} \tag{20}$$

Therefore, the next step is to extract the ripple voltage component $\tilde{V}^e_{ds\_fb}$ from the d-axis current controller output voltage $V^e_{ds\_fb}$. To do this, the feedback d-axis current i^e_{ds} is then filtered through a bandstop filter to attenuate its injected ripple content and the center frequency of which is adequately tuned to the injected frequency ω_h. The error signal between optimal d-axis current $i^{e^*}_{ds}$ and bandstop filtered current feeds a proportional–integral (PI) controller which has the same structure and bandwidth as a main PI current controller. Then, as can be seen from Fig. 6, the output voltage of PI controller corresponds to the flux-weakening controller voltage component $V^e_{ds\_fb1}$. From the difference between d-axis current controller output voltage and flux-weakening controller voltage component, the ripple voltage component

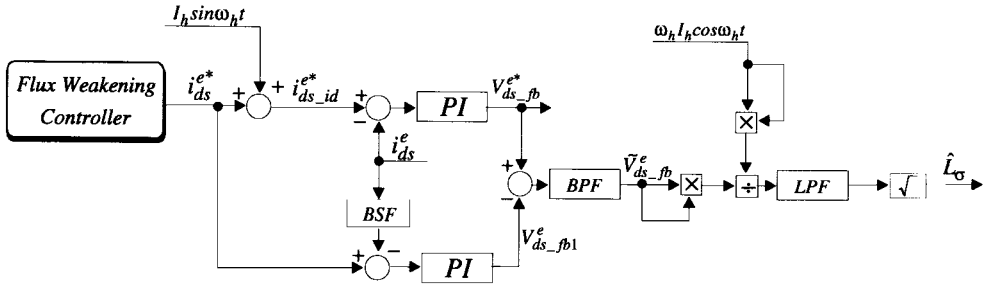

Fig. 7. Configuration of stator transient inductance estimator.

$\tilde{V}_{ds\_fb}^{e}$ can be calculated as

$$\tilde{V}_{ds\_fb}^{e} = L_\sigma \frac{d\tilde{i}_{ds}^{e}}{dt} = V_{ds\_fb}^{e} - V_{ds\_fb1}^{e}. \tag{21}$$

Equation (21) can be rewritten as

$$(\tilde{V}_{ds\_fb}^{e} - (R_s + R_r)\tilde{i}_{ds}^{e})^2 = \omega_h^2 L_\sigma^2 I_h^2 \frac{1+\cos 2\omega_h t}{2}. \tag{22}$$

Eliminating the $\cos 2\omega_h t$ term by applying a low-pass filter to (22), the stator transient inductance can be obtained as

$$\hat{L}_\sigma = \sqrt{\frac{2LPF[(\tilde{V}_{ds\_fb}^{e} - (R_s + R_r)\tilde{i}_{ds}^{e})^2]}{\omega_h^2 I_h^2}}. \tag{23}$$

Therefore, the value of the stator transient inductance is uniquely identified from the ripple voltage content $\tilde{V}_{ds\_fb}^{e}$. In this scheme, because $\tilde{V}_{ds\_fb}^{e}$ is nearly equal to the voltage drop of leakage inductances, the estimated stator transient inductance is insensitive to both stator and rotor resistance. This technique is suitable for covering all operating conditions because the excitation frequency is selected to reduce skin effect as (18). Thus, maximum torque control can be performed over all operating conditions including steady state and transient state. The overall configuration of estimator is shown in Fig. 7.

VI. Simulation Results

In order to verify the feasibility of the proposed algorithm, computer simulation has been carried out. A 22-kW induction machine is used in the simulation, and the ratings and parameters of the machine are shown in Table I. The switching device is assumed to be an insulated gate bipolar transistor (IGBT) of 3-kHz switching frequency and the dc-link voltage is 280 V considering the dead-time effect. The maximum stator current $I_{s\ \max}$ is 130 A which corresponds to 150% of the rated current of the test machine. The sampling period of current and speed control is 167 μs and 2 ms, respectively, and the cutoff frequency of the current and speed controller is selected to 2000 and 150 rad/s, respectively.

To analyze the stability of proposed flux-weakening algorithm, the small-signal analysis is performed about an operating point. Equations (24)–(27) show the nature of the nonlinear features of the induction machine represented in the stationary reference frame

$$p\vec{i}_{qds}^{s} = \frac{1}{L_\sigma}\left(\vec{v}_{qds}^{s} - r_s'\vec{i}_{qds}^{s} + \frac{L_m}{L_r}\omega_{br}\vec{\lambda}_{qdr}^{s}\right) \tag{24}$$

$$p\vec{\lambda}_{qdr}^{s} = \frac{L_m}{\tau_r}\vec{i}_{qds}^{s} - \omega_{br}\vec{\lambda}_{qdr}^{s} \tag{25}$$

$$T_e = \frac{3}{2}\frac{P}{2}\frac{L_m}{L_r}(\vec{i}_{qds}^{s} \otimes \vec{\lambda}_{qdr}^{s}) \tag{26}$$

$$p\omega_{rm} = \frac{1}{J_m}(T_e - B_m\omega_{rm} - T_l) \tag{27}$$

where $\omega_{br} = (1/\tau_r) - j\omega_r$, $r_s' = r_s + r_r(L_m^2/L_r^2)$, and $\otimes$ denotes a vector cross product. The induction machine model is seen to be nonlinear due to the products of variables (flux and speed for induced voltages, and flux and current for torque). It is widely known that a nonlinear system should behave similarly to its linearized approximation around an equilibrium point [12]. Therefore, the nonlinear model can be linearized using small-signal model which is represented in the synchronous reference frame as in (28)–(31) [13]. This linearized model serves as the fundamental justification of using linear control techniques (e.g., root locus method) in practice, i.e., shows that stable design by linear control guarantees the stability of the original physical system locally

$$p\Delta\vec{i}_{qds}^{e} = \frac{1}{L_\sigma}(\Delta\vec{v}_{qds}^{e} - (r_s' + j\omega_e L_\sigma)\Delta\vec{i}_{qds}^{e} + \frac{L_m}{L_r}(\omega_{bro}\Delta\vec{i}_{qdr}^{e} - j\vec{I}_{qdro}^{e}\Delta\omega_r)) \tag{28}$$

$$p\Delta\vec{\lambda}_{qds}^{e} = \frac{L_m}{\tau_r}\Delta\vec{i}_{qds}^{e} - (\omega_{bro} + j\omega_e)\Delta\vec{\lambda}_{qdr}^{e} + j\vec{\lambda}_{qdro}^{e}\Delta\omega_r \tag{29}$$

$$p\Delta T_e = \frac{3}{2}\frac{P}{2}\frac{L_m}{L_r}(\Delta\vec{i}_{qds}^{e} \otimes \vec{\lambda}_{qdro}^{e} + \vec{i}_{qdso}^{e} \otimes \Delta\vec{\lambda}_{qdr}^{e}) \tag{30}$$

$$p\Delta\omega_{rm} = \frac{1}{J_m}(\Delta T_e - B_m\Delta\omega_{rm} - \Delta T_l) \tag{31}$$

where subscript o' denotes the steady-state data.

To analyze the stability of proposed controller, the steady-state data are used which consist of rotor flux and stator current, and mechanical speed obtained from the proposed flux-weakening algorithm. Such information is useful in the analysis of machine instability which results when an induction machine is driven from a control algorithm. Using the data in the proposed algorithm at steady state, a plot of the corresponding system poles is shown in Fig. 8. In Fig. 8, the poles are

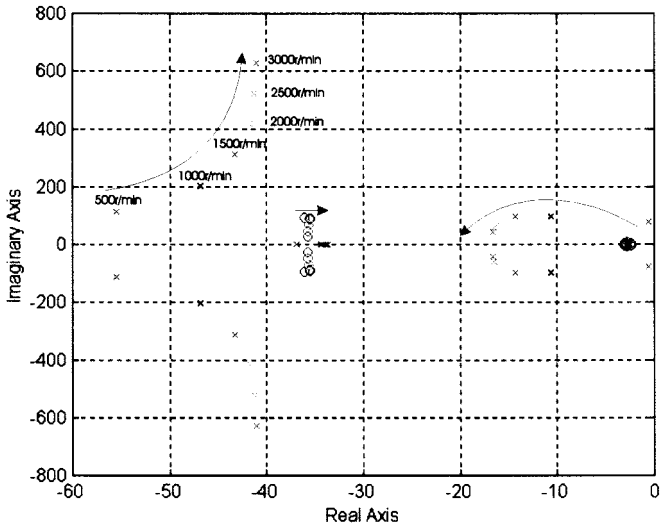

Fig. 8. Plot of system poles according to speed change.

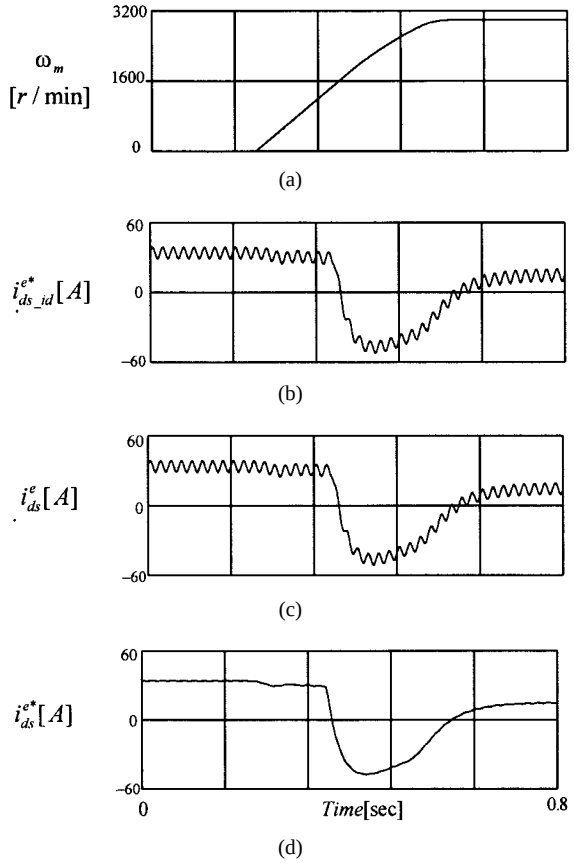

Fig. 9. Starting transient for induction machine under test: (a) machine actual speed, (b) d-axis current command, (c) d-axis feedback current, and (d) calculated optimal d-axis current.

marked $\boldsymbol{x}$ and the zeros are $\boldsymbol{o}$. The mechanical speed is changed from 500 to 3000 r/min. From this analysis, it can be observed that all system poles and zeros are located in left-half plane under control conditions and the proposed controller is locally stable around an equilibrium point. Therefore, practically and empirically, it can be concluded that the proposed controller is stable over all flux-weakening region.

Fig. 9 shows the transient responses of mechanical speed, d-axis current command $i^{e*}_{ds\_id}$, feedback current i^{e}_{ds}, and

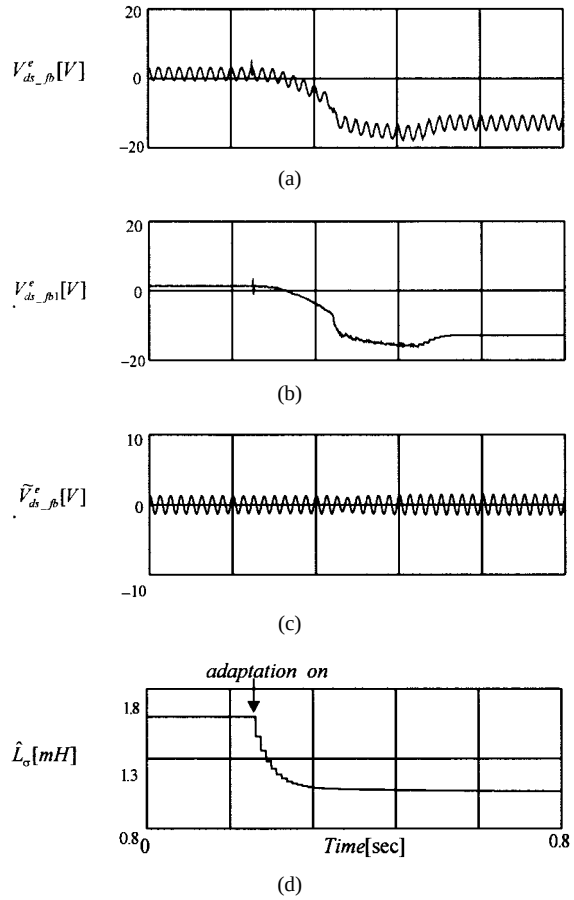

Fig. 10. Estimation characteristic of stator transient inductance: (a) d-axis current controller output voltage, (b) flux-weakening controller voltage component, (c) ripple voltage component, and (d) estimated stator transient inductance.

calculated optimal d-axis current from top to bottom. In order to reduce skin effect, the injected signal frequency and amplitude is selected as 50 Hz and 5 A. With this excitation frequency, the inequality condition (18) is satisfied and the skin effect is minimized as shown in Fig. 4. The center frequency of the bandstop filter is set to the injected frequency of 50 Hz. The bandstop filter introduced a phase shift in the filtered signal current, which created a small but not noticeable error in the estimation of stator transient inductance. The speed command changes from 0 to 3000 r/min at 0.2 s. In this test, the machine speed does not reach the onset speed of region II. To reduce the rotor flux level according to speed increase, the d-axis current decreases at onset of flux-weakening region I.

In Fig. 10, the d-axis current controller output voltage $V^{e}_{ds\_fb}$, flux-weakening controller voltage component $V^{e}_{ds\_fb1}$, ripple voltage component $\tilde{V}^{e}_{ds\_fb}$, and estimated stator transient inductance $\hat{L}_\sigma$ are illustrated from top to bottom. As the mechanical speed increases, the d-axis output voltage $V^{e}_{ds\_fb}$ with ripple component decreases to control d-axis current i^{e}_{ds} as shown in Fig. 10(a). At the initial point, the value of stator transient inductance is 1.6 mH which corresponds to 143% of actual value 1.1 mH. When the adaptation is activated, it is found that the value of estimated stator transient inductance

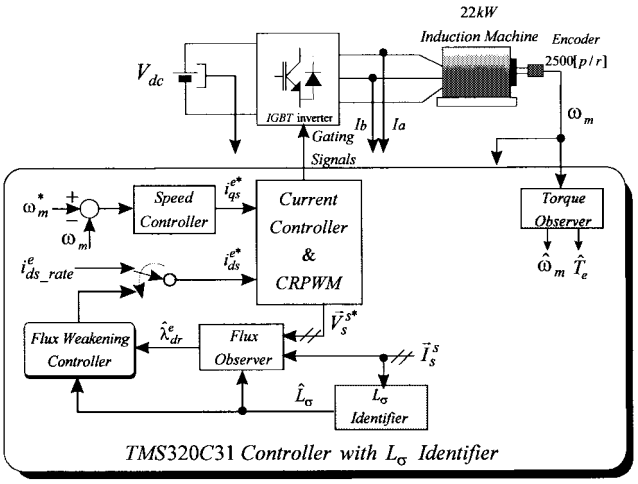

Fig. 11. Experimental system configuration.

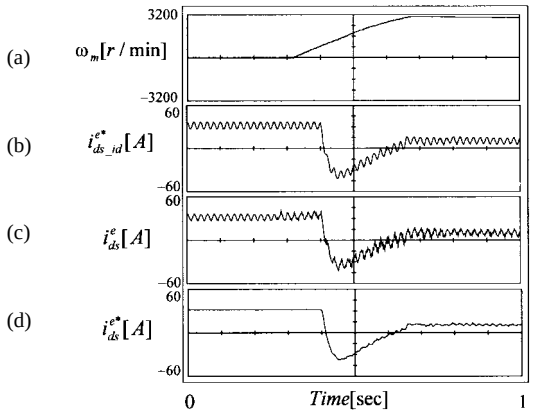

Fig. 12. Starting transient for induction machine under test: (a) machine actual speed, (b) d-axis current command, (c) d-axis feedback current, and (d) calculated optimal d-axis current.

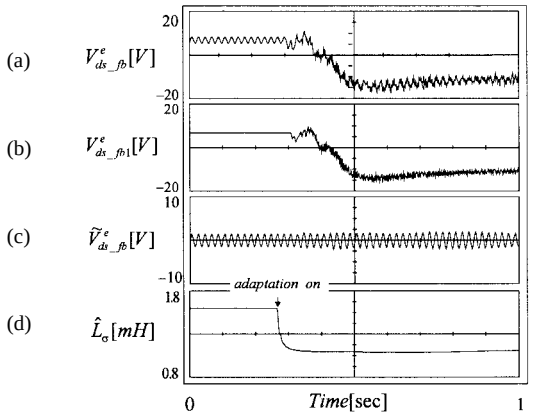

Fig. 13. Estimation characteristic of stator transient inductance: (a) d-axis current controller output voltage, (b) flux-weakening controller voltage component, (c) ripple voltage component, and (d) estimated stator transient inductance.

is in acceptable range compared to actual value though the d-axis voltage and current are varying for the flux-weakening operation. In trace (d) at the bottom, the tracking performance is illustrated and the estimated value converges to actual value in about 120 ms. The test result shows that the identified value is reasonably accurate and the percentage difference between the actual and estimated value is within -5%.

VII. Experimental Results

Extensive tests are performed to evaluate the feasibility of the presented study. The algorithm is programmed and installed on actual IGBT inverter to drive 22-kW induction machine. The overall experimental setup is shown in Fig. 11.

The switching devices in the inverter are IGBT's with 3-kHz switching frequency. The dc-link voltage is 300 V and the sampling period of current control is 167 μs. Using the space vector PWM scheme with dead-time compensator, the terminal voltage measurement is not required, thus, the output voltage sensors are not used. TMS320C31 DSP is used as a main control processor, which operates with 33.33-MHz clock and is capable of 33.33 mega floating point operations per second.

In order to ensure the validity of the proposed algorithm, it is required to measure the actual machine torque. An ideal method would be to calculate the torque by differentiating the mechanical speed, but direct differentiation enlarges the noise component. Therefore, the torque observer is designed to monitor the actual torque [14]. The sampling time of speed detection is about 2 ms, and the observer is designed to have 100-Hz cutoff frequency. The measurement speed error for the worst case is less than 0.35 r/min at 3000 r/min, and this error corresponds to about 3 Nm or 0.026 per unit (p.u.) of rated torque. To examine the estimation characteristic of stator transient inductance, some tests are performed on a 22-kW machine with the speed reference from standstill to 3000 r/min. The running conditions are identical to the conditions in simulation.

In order to reduce skin effect, the injected signal frequency and amplitude is selected as 50 Hz and 5 A. The additional voltage for the control of injection current can be calculated using machine parameters as

$$V_{\text{add}} = (R_s + R_r)I_h + \omega_h L_\sigma i_H. \tag{32}$$

The additional voltage in the case of experimental setup is 5 V, which is less than 3% of the possible inverter output voltage. Therefore, the current controller instability problems from this additional voltage can be neglected. For a large machine, it is evident that the skin effect might be severe compared to that of small machine. In this case, to reduce the estimation error the lower frequency signal should be appropriately used.

Fig. 12 shows the transient responses of mechanical speed, d-axis current command $I_{ds\_id}^{e^*}$, feedback current i_{ds}^{e}, and optimal d-axis current $i_{ds}^{e^*}$ from top to bottom. It can be observed from these waveforms that the d-axis current decreases at onset of flux-weakening region I. Unlike the simulation results, the feedback current has some noise components which is due to the current and speed sensor, time delay, and estimated rotor flux. In Fig. 13, d-axis current controller output voltage $V_{ds\_fb}^{e}$, flux-weakening controller voltage component $V_{ds\_fb1}^{e}$, ripple voltage component $\tilde{V}_{ds\_fb}^{e}$, and estimated stator transient inductance $\hat{L}_\sigma$ are illustrated from top to bottom. Due

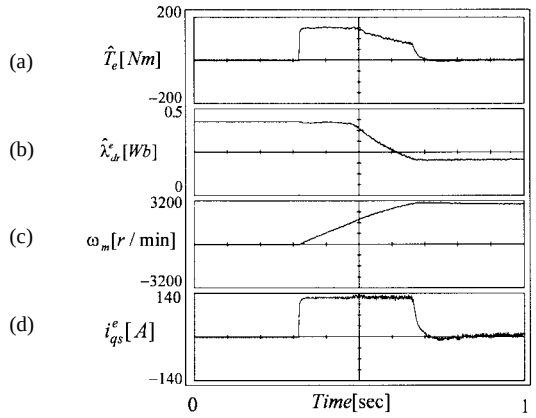

Fig. 14. Dynamic response in step speed command: (a) estimated torque, (b) estimated rotor flux, (c) actual mechanical speed, and (d) q-axis actual current.

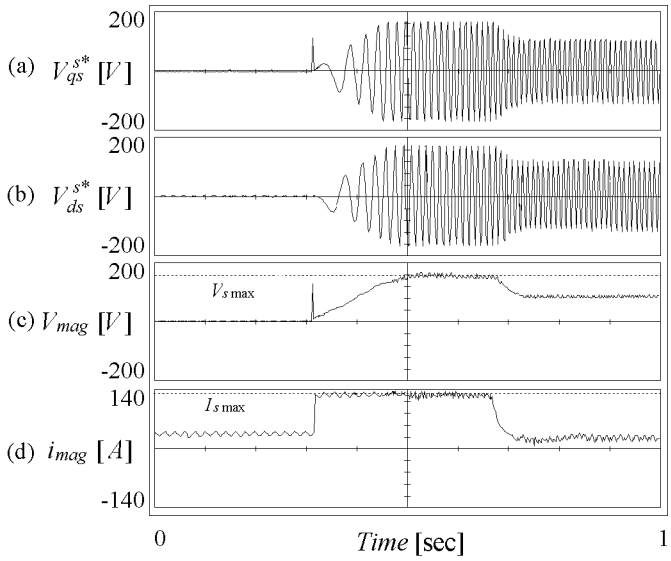

Fig. 15. Voltage and current magnitude of proposed algorithm: (a) q-axis voltage in stationary frame, (b) d-axis voltage in stationary frame, (c) magnitude of controller output voltage vector, and (d) magnitude of controlled current vector.

to the noise in measured current signal, $V^e_{ds\_fb}$ and $V^e_{ds\_fb1}$ have some degree of high-frequency ripple in addition to the injected 50-Hz ripple content. The high-frequency noise components do not appear in the ripple voltage component $\tilde{V}^e_{ds\_fb}$ because $\tilde{V}^e_{ds\_fb}$ is the difference voltage between $V^e_{ds\_fb}$ and $V^e_{ds\_fb1}$. This means that the proposed estimation scheme is inherently immune to the system noise. At the initial point, the value of stator transient inductance is 1.6 mH which corresponds to 143% of tuned value. When the adaptation is activated, it is found that the value of estimated stator transient inductance is reasonably accurate compared to tuned value 1.1 mH, though the d-axis voltage and current are varying for the flux-weakening operation.

Fig. 14 shows the transient responses of optimal flux-weakening controller with stator transient inductance identifier. In this test, the rotor flux quantity is estimated through the rotor flux observer and the torque is estimated from torque observer. Selecting optimal rotor flux level of an induction machine, excellent dynamic performance can be achieved in overall speed region.

Fig. 15 shows the experimental results when the machine is accelerated from 0 to 3000 [r/min] with 1.5 times of the rated current. Fig. 15(a) and (b) shows the q- and d-axis voltages in stationary reference frame that are controlled according to the voltage pattern for maximum torque operation. In Fig. 15(c), $V_{\rm mag}$ denotes the magnitude of controller output voltage vector and it is seen that the drive system fully utilizes the possible inverter output voltage $V_{s\ \max}$ in the flux-weakening region. Fig. 15(d) shows the magnitude of controlled current vector $i_{\rm mag}$. From this waveform, it is observed that all the current controllers fully use their control voltage in transient region keeping the optimal flux level.

VIII. Conclusions

A stator transient inductance estimation scheme to guarantee the performance of high-speed operation of an induction machine has been proposed and verified in this paper. Based on the injection of sinusoidal current, the adaptation procedure is insensitive to parameters of machine and intends to reduce the adverse effects of skin effect on the estimation of the stator transient inductance. The proposed scheme has been shown to perform effectively under conditions of constant and variable speeds. Also, the detuned effect of machine inductance is thoroughly analyzed to relate the sensitivity of parameters to the operation of flux-weakening region. Simulation and experimental results demonstrate that the proposed adaptation scheme effectively combines the optimal flux selection with accuracy of stator transient inductance.

References

[1] S.-H. Kim and S.-K. Sul, "Voltage control strategy for maximum torque operation of an induction machine in the field weakening region," *IEEE Trans. Ind. Electron.*, vol. 44, pp. 512–518, Aug. 1997.

[2] H. Grotstollen and J. Wiesing, "Torque capability and control of a saturated induction motor over a wide range of flux weakening," *IEEE Trans. Ind. Electron.*, vol. 42, pp. 374–381, Aug. 1995.

[3] S.-H. Kim and S.-K. Sul, "Maximum torque control of an induction machine in the field weakening region," *IEEE Trans. Ind. Applicat.*, vol. 31, pp. 787–794, July/Aug. 1995.

[4] M. Bodson, J. N. Chiasson, and R. T. Novotnak, "A systematic approach to selecting flux references for torque maximization in induction motors," *IEEE Trans. Contr. Syst. Technol.*, vol. 3, pp. 388–397, Dec. 1995.

[5] J.-K. Seok and S.-K. Sul, "Optimal flux selection of an induction machine for torque maximization," in *IEEE Int. Electrical Machine and Drive Conf. (IEMDC)*, 1997, pp. TB3-2.1–TB3-2.3.

[6] P. Vas, *Parameter Estimation, Condition Monitoring, and Diagnosis of Electrical Machines*. Oxford, U.K.: Oxford Science, 1993.

[7] J.-K. Seok, S.-I. Moon, and S.-K. Sul, "Induction machine parameter identification using PWM inverter at standstill," *IEEE Trans. Energy Conversion*, vol. 12, pp. 127–132, June 1997.

[8] R. J. Kerkman, J. D. Thunes, T. M. Rowan, and D. W. Schlegel, "A frequency-based determination of transient inductance and rotor resistance for field commissioning purposes," *IEEE Trans. Ind. Applicat.*, vol. 32, pp. 577–584, May/June 1996.

[9] P. L. Jansen and R. D. Lorenz, "Tranduceless field orientation concepts employing saturation-induced saliences in induction machines," *IEEE Trans. Ind. Applicat.*, vol. 10, pp. 1380–1393, Nov./Dec. 1996.

[10] S.-I. Yong, J.-W. Choi, and S.-K. Sul, "Sensorless vector control of induction machine using high frequency current injection," in *IEEE Industry Applications Soc. Annu. Meeting*, 1994, pp. 503–508.

[11] T. Noguchi, S. Kondo, and I. Takahashi, "Field-oriented control of an induction motor with robust on-line tuning of its parameters," *IEEE Trans. Ind. Applicat.*, vol. 33, pp. 35–42, Jan./Feb. 1997.

[12] J.-J. E. Slotine and W. Li, *Applied Nonlinear Control*. Englewood Cliffs, NJ: Prentice-Hall, 1991, pp. 40–75.
[13] D. E. Borgard, G. Olsson, and R. D. Lorenz, "Accuracy issues for parameter estimation of field oriented induction machine drives," *IEEE Trans. Ind. Applicat.*, vol. 31, pp. 795–801, July/Aug. 1995.
[14] S.-J. Kang and S.-K. Sul, "Direct torque control of brushless dc motor with nonideal trapezoidal back EMF," *IEEE Trans. Power Electron.*, vol. 10, pp. 796–802, Nov. 1995.

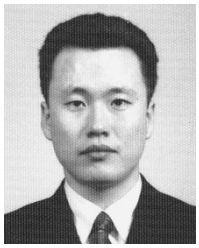

Jul-Ki Seok (S'94) was born in Pusan, Korea, in 1969. He received the B.S., M.S., and Ph.D. degrees in electrical engineering from Seoul National University, Seoul, Korea, in 1992, 1994, and 1998, respectively.

He is with the Production Engineering Center, Samsung Electronics Company Ltd., Suwon City, Korea. His specific research interests are in electrical machines, high-performance electrical machine drives, and high-power ac drives. Currently, he works on high-speed CNC machine tools and an open servo drive system.

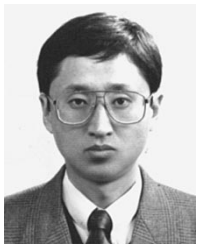

Seung-Ki Sul (S'78–M'87) was born in Pusan, Korea, in 1958. He received the B.S., M.S., and Ph.D. degrees in electrical engineering from Seoul National University, Seoul, Korea, in 1980, 1982, and 1986, respectively.

He was with the Department of Electrical Engineering, University of Wisconsin, Madison, as a Visiting Research Associate from 1986 to 1988. From 1988 to 1990, he was with the GoldStar Industrial Systems Company, Seoul, as a Principal Research Engineer. Since 1991, he has been a Faculty Member in the School of Electrical Engineering, Seoul National University, serving as an Associate Professor. His present research interests are in high-performance electric machine control, electric vehicle drives, and power converter circuits. He is performing various research projects for industrial systems, and some of the results are being applied to the fields of industrial high-power electric machine control.